

Extreme Isotopic Fractionation in CO and H₂ Formed in Formaldehyde Photolysis: Theory and Experiment

Luisa Pennacchio, Zacharias Liasi, Andreas Erbs Hillers-Bendtsen, Thomas Röckmann, Kurt V. Mikkelsen, and Matthew S. Johnson*



Cite This: <https://doi.org/10.1021/acs.jpca.4c07516>



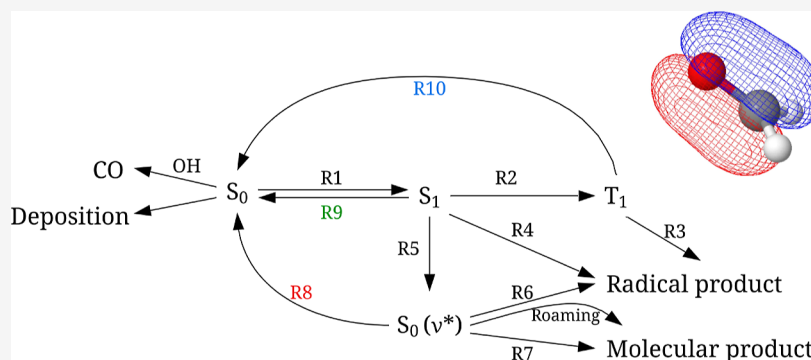
Read Online

ACCESS |

Metrics & More

Article Recommendations

Supporting Information



ABSTRACT: Formaldehyde (HCHO) is an important intermediate in the breakdown of organic molecules in the atmosphere. It is the most abundant atmospheric carbonyl, and a major source of CO and H₂ upon degradation. Isotopic analysis offers valuable insights into molecular processes, deepening our understanding of atmospheric transformations. We present a model of the isotope-dependent photolytic isotopic fractionation of formaldehyde incorporating Rice–Ramsperger–Kassel–Marcus (RRKM) analysis, validate the model with new and pre-existing experimental data, and use it to describe photolytic kinetic isotope effects (KIEs) and their pressure dependencies. RRKM theory was used to calculate decomposition rates of the S₀, S₁, and T₁ states, using CCSD(T)/aug-cc-pVTZ, ωB97X-D/aug-cc-pVTZ, and CASPT2/aug-cc-pVTZ, respectively. We considered isotopologues HCHO, DCHO, DCDO, D¹³CHO, H¹³CHO, HCH¹⁷O, HCH¹⁸O, H¹³CH¹⁷O, and H¹³CH¹⁸O. We find that isotopic substitution notably affects the density of states, influencing rates of unimolecular decomposition and collisional energy transfer. Experimental photolysis rates ranged from $j_{\text{HCHO}}/j_{\text{HCH}^{18}\text{O}} = 1.027 \pm 0.006$ at 50 mbar to $j_{\text{HCHO}}/j_{\text{DCDO}} = 1.418 \pm 0.108$ at 1000 mbar using a xenon lamp. The model accurately reproduced experimental pressure trends in KIEs, revealing that altitude-dependent deuterium enrichment in H₂ cannot be explained by pressure effects alone and must also consider wavelength dependence.

INTRODUCTION

Formaldehyde (HCHO) is the most abundant carbonyl compound in the atmosphere and is a key intermediate produced in the oxidation of virtually all hydrocarbons. It is a major in situ source of atmospheric molecular hydrogen and carbon monoxide. In addition to photochemical production, formaldehyde is emitted directly into the atmosphere from combustion. Because formaldehyde is a reactive species and an important part of both natural and anthropogenic atmospheric chemistry, understanding its photochemistry is important for regional air quality, global atmospheric composition and climate change.¹

The importance of HCHO is illustrated by the finding that over half of atmospheric H₂ is produced from the photolysis of HCHO.^{2–5} Molecular hydrogen is the reduced gas in the atmosphere with the largest turnover in moles and acts as an indirect greenhouse gas.⁶ Interest in H₂ has increased in recent

years due to its use as a carbon-free energy carrier. Widespread adaptation would increase H₂ emissions due to leaks in production, storage, distribution and use.^{7–11} Understanding the natural atmospheric H₂ cycle in more detail is therefore essential to assess the impact of a future hydrogen economy.¹²

Approximately half of tropospheric carbon monoxide (CO) is produced from the oxidation of hydrocarbons, where HCHO is the key intermediate.^{13,14} All reaction pathways for HCHO with the exception of deposition lead to the formation of CO. The reaction of CO with OH radicals accounts for 40%

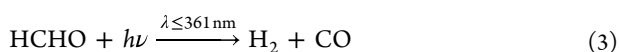
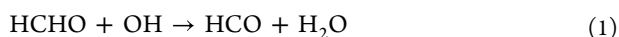
Received: November 5, 2024

Revised: February 1, 2025

Accepted: February 4, 2025

of the removal of OH in the troposphere.¹⁵ As such, HCHO plays a key role in the oxidative capacity and HOx chemistry of the atmosphere, and in modulating the indirect climate effect of volatile organic compounds. Formaldehyde contributes to secondary organic aerosol formation in reactions catalyzed by sulfuric acid.¹⁶

The primary removal pathways for HCHO in the troposphere are reactions with photochemically produced radicals (Reaction 1), photolysis (Reactions 2 and 3) and deposition. It is estimated that during daytime, photolysis and the radical reaction are of approximately equal importance, depending on altitude and location. Globally, OH is by far the most important radical, but Cl radicals can play an important role in certain environments, such as the marine boundary layer.^{1,17}



The UV spectrum of formaldehyde is highly structured.^{18–21} The electronic dipole forbidden $S_1 \leftarrow S_0$ transition becomes allowed through vibronic coupling at wavelengths starting at 380 nm.¹⁸ The quantum yields of the radical channel (Reaction 2) and the molecular channel (Reaction 3) are wavelength and pressure dependent. Under most tropospheric conditions, the molecular channel is somewhat larger than the radical channel.²²

Figure 1 shows the key elementary processes for the photoexcitation and photodissociation of formaldehyde.^{23–26}

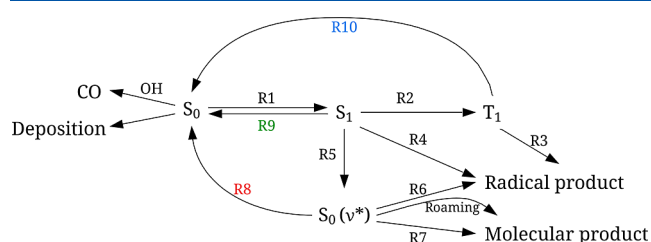


Figure 1. Present understanding of the photolytic breakdown of formaldehyde from the atmosphere. S_0 , S_1 and T_1 are electronic states, $S_0(\nu^*)$ is the vibrationally excited ground state and R2 is ISC, R5 is IC, and R8, R9, and R10 are collisional quenching.

Reaction R1 is photoexcitation from the ground state S_0 to the singlet excited state S_1 . This state can undergo intersystem crossing (ISC) to the triplet state T_1 in R2, which can fall apart into the radical products H and HCO in reaction R3. Alternatively, S_1 itself can fall apart into the radical products via R4. The S_1 state could undergo internal conversion (IC) to form a vibrationally hot molecule on the ground state surface,

via R5, written $S_0(\nu^*)$. This state could decay into the radical products in R6. Experiments have shown that the molecular products CO and H_2 are only produced from the S_0 surface in R7, at energies above a threshold corresponding to a photon wavelength shorter than 360 nm. The molecular products can also be formed in a process that begins in the radical channel. A hydrogen atom travels around the carbonyl group and abstracts hydrogen from the formyl radical, bypassing the transition state for the molecular product.²⁷ This minor path has not been included in this study. Finally, the three processes R8, R9, and R10 represent collisional quenching of $S_0(\nu^*)$, S_1 and T_1 respectively. The rate of energy transfer depends on the density of states and therefore the isotopic composition and internal energy, and for R10, the coupling between T_1 and S_0 .

The model was run at 1030 mbar and average sea level actinic flux at the coordinates of EUPHORE the 17-06-2007 from 8:00 to 12:00.

Isotopic analysis can provide insight into many atmospheric mechanisms, as trace gas sources have distinguishable isotopic abundances and production and loss mechanisms have unique isotopic fractionations. Isotopic substitution changes vibrational frequencies, thereby changing zero point energies, impacting the activation energy, partition functions, the probability of reaction and the density of states. Clearly, there are also mass and symmetry dependent changes in reaction dynamics. Isotopic substitution results in changed rates of the elementary processes shown in Figure 1 and thereby different lifetimes for the excited states of the isotopologues. The kinetic isotope effects (KIEs) in the photolysis of formaldehyde under ambient conditions, for DCHO, DCDO, H^{13}CHO and HCH^{18}O , have been determined in several studies and are summarized in Table 1. Gratien et al.¹⁹ found that the isotopic changes in the integrated UV absorption cross sections of formaldehyde and its deuterated species (i.e., positions and intensities of vibrational structure components convoluted with the excitation spectrum) are equal within the experimental uncertainty; however, the differences in the vibronic structures are large enough that this should be taken into account when calculating the excitation rate (see Figure 2).

There is a significant body of research concerning the chemical dynamics of formaldehyde photolysis. Many processes are involved: intersystem crossing, internal conversion, unimolecular dissociation, collisional quenching, chemical reaction and direct dissociation.³³ Initial experiments by Houston and Moore³⁴ indicated the presence of a long-lived intermediate state between S_1 and the CO and H_2 products. However, subsequent work found that the delay was in fact CO detection, not production. The CO product was produced in a highly rotationally excited state, resulting in a delay as the CO was slowly quenched.^{33,35} In the context of this work, the excited state is nonetheless quite long-lived, long

Table 1. Summary of Previous Experimental Results for the Isotope Effects in Formaldehyde Photolysis at Atmospheric Pressure and the Kinetic Isotope Effect, $\alpha = j_{\text{light}}/j_{\text{heavy}}$ Obtained Using the Model

	model sunlight	Feilberg ^{28,29} EUPHORE sunlight	Nilsson ³⁰ EURPHORE sunlight	Röckmann ³ SAPHIRE Sunlight	Rhee ⁵ Duran sunlight	model UVA	Nilsson ^{31,32} quartz UVA
HCDO	1.319 ± 0.132	1.58 ± 0.03		1.63 ± 0.03	2.50 ± 0.17	1.383 ± 0.138	1.75 ± 0.1
DCHO	1.610 ± 0.161					1.735 ± 0.174	
DCDO	2.186 ± 0.219	3.003 ± 0.607	3.15 ± 0.08			2.682 ± 0.268	3.16 ± 0.03
H^{13}CHO	1.007 ± 0.101	1.195 ± 0.334				1.012 ± 0.101	
HCH^{18}O	0.999 ± 0.100	1.205 ± 0.338				0.999 ± 0.100	

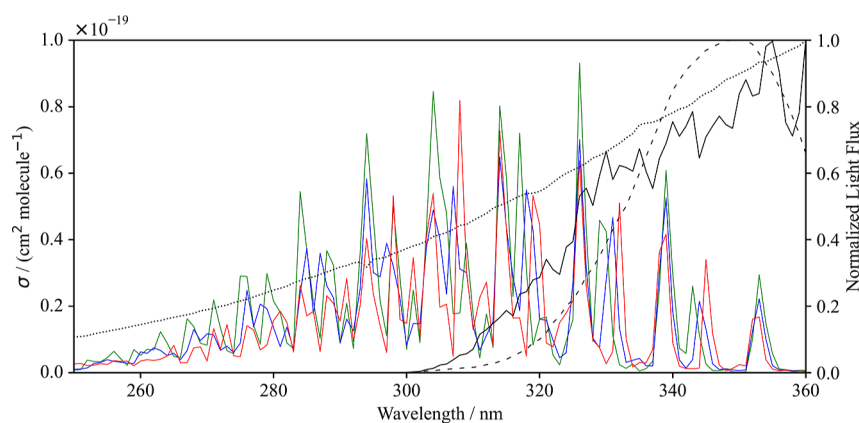


Figure 2. Absorption cross-section, σ , of HCHO (green), DCHO (blue) and DCDO (red) from Gratien et al.,¹⁹ emission spectrum of Eimac xenon lamp (dotted line), emission spectrum of UV-A Osram Eversun lamp (dashed line) used by Nilsson et al.,^{31,32} and solar spectrum at ground level (black).

enough for intersystem crossing and internal conversion to take place. In their predissociation model, Yeung and Moore³⁶ found the behavior of formaldehyde to be consistent with a two-step process wherein the excited state is more strongly coupled to the continuum than to the ground state. Using Stark level-crossing spectroscopy, Polik et al.³⁷ found that S_1 – S_0 coupling matrix elements vary from 3.5×10^{-7} to $4.7 \times 10^{-5} \text{ cm}^{-1}$ showing that the behavior of neighboring eigenstates can vary dramatically. They found that the barrier height for unimolecular dissociation on the S_0 DCDO surface is $335 \pm 3.4 \text{ kJ/mol}$ ($331 \pm 3.3 \text{ kJ/mol}$ for HCHO). In an analysis of the thermal dissociation of formaldehyde, Troe found a barrier of $E_{0,1} = 342 \pm 0.5 \text{ kJ/mol}$.³⁸ A molecular beam experiment by Ho et al.³⁵ excited HCHO near the S_1 origin. Detection of CO gave strong support to the sequential coupling model for fast nonradiative decay of S_1 states through broadened S_0 levels to the continuum. Similarly, Weisshaar and Moore³⁹ found that the lifetimes of single rovibronic levels of S_1 HCHO and DCDO vary from 20 ns to 3.1 μs , which is explained using a sequential decay mechanism, $S_1 \rightarrow S_0 \rightarrow \text{H}_2(\text{D}_2) + \text{CO}$. They note that the last state could involve tunneling at lower excitation energies. Recently, a new mechanism was described in which vibrationally hot formaldehyde in the ground state reacts with O_2 to yield HCO and HO_2 .⁴⁰

Broadband photolysis, such as solar or lamp photolysis, averages over a multitude of states. In previous work, the KIE for broadband formaldehyde photolysis was calculated for the S_0 state using an RRKM model. This approach could only explain roughly half of the observed isotope effect.³² In this paper, we build a model based on elementary photochemical processes to explain the photolytic KIE. The model predicts the KIEs of a series of isotopologues as a function of energy, pressure and temperature. We validate the model using all available and new experiments, and use it to predict isotope effects under a wide range of conditions.

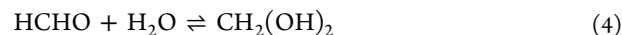
In the following three sections, we provide the experimental, computational and theoretical details. We then present the results and discussion, followed by the prediction made with the model, and finally, offer our conclusions.

EXPERIMENTAL DETAILS

Photolysis experiments were carried out in a multipass cell from Infrared Analysis, Inc. with a volume of 2.3 L and an analytical path length of 13.40 m. A UV-transparent window

was installed at the top of the cell where an Eimac xenon lamp was mounted. The emission spectrum of the lamp is shown in Figure 2 (dotted line). The cell was mounted in a Vertex 70 Fourier Transform Infrared (FTIR) spectrometer. The infrared spectra were obtained by averaging 60 interferograms with a spectral resolution of 0.50 cm^{-1} , an aperture setting of 6 mm, a scanner velocity of 60 kHz (9.5 mm/s) and a liquid-nitrogen-cooled InSb detector.

The relative photolysis rates of HCHO versus DCHO, DCDO, H^{13}CHO or HCH^{18}O were determined at nominal total pressures of 50, 200, 500, and 1000 mbar using N_2 as bath gas. Gas-phase samples were prepared by heating paraformaldehyde, and transferred to the photolysis cell using a gas line. Paraformaldehyde- ^{18}O was synthesized from paraformaldehyde (natural isotopic abundance) and ^{18}O -labeled water, using the rapid exchange



Paraformaldehyde and ^{18}O -labeled water (Campro Scientific, >95 atom % ^{18}O) were attached to the gas line where the ^{18}O -labeled water was placed in a cold trap containing liquid nitrogen. The paraformaldehyde was heated, and the resulting gas-phase formaldehyde was captured in the cold trap with the ^{18}O -labeled water. The sample was closed off from the gas line, the cold trap was removed and the solution was allowed to equilibrate for 24 h, after which the water vapor was pumped off, leaving ^{18}O -labeled paraformaldehyde.

Approximately 0.7 mbar of HCHO and a substituted isotopologue were introduced into the cell, which was then filled with bath gas to the desired total pressure. The multipass cell was closed off, and a spectrum was taken in the range 600 – $10,000 \text{ cm}^{-1}$. The light source was then turned on in five-minute intervals, followed by recording spectra for a total of at least 45 min, except for HCHO/DCHO, which was determined at a single point after 30 min of irradiation. The peaks used for analysis were the $\text{C}=\text{O}$ overtones located between 3380 and 3540 cm^{-1} . Using the subtraction tool in the software program OPUS,⁴¹ the spectrum after light exposure was manually subtracted from the spectrum before exposure, yielding the extent of reaction. The relative rates could thus be determined using

$$\frac{j}{j'} = \frac{\ln([R]_0/[R]_t)}{\ln([R']_0/[R']_t)} \quad (5)$$

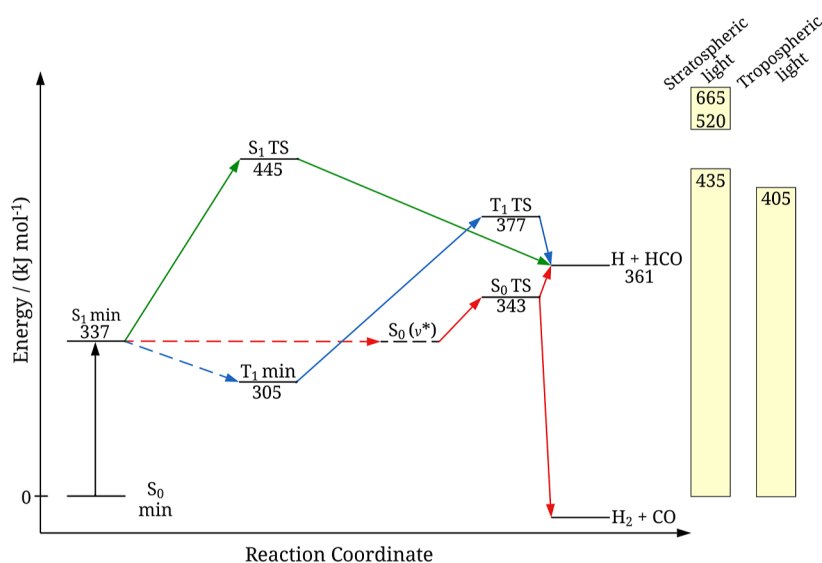


Figure 3. Stationary state energies for HCHO, TS is “transition state”. The energies are averages from literature values.^{23–27,33,50–58} The $S_0(v^*)$ state is marked with dashed lines, as the energy is dependent on the incoming energy. The yellow bars illustrate the energy of the light available in the stratosphere and troposphere.

where j and j' are the photolysis rates of HCHO and an isotopologue, $[R]_0$ and $[R]_t$ are the concentrations of HCHO at time 0 and at time t , and similarly for the isotopologue.

COMPUTATIONAL DETAILS

Geometry optimizations and frequency calculations were performed for the reactants, transition states and products for reactions R2–R7 (see Figure 3) for the following isotopologues: HCHO, HCDO, DCHO, DCDO, $H^{13}CDO$, $D^{13}CHO$, $H^{13}CHO$, $HCH^{17}O$, $HCH^{18}O$, $H^{13}CH^{17}O$ and $H^{13}CH^{18}O$. Two distinct reaction pathways exist for the monodeuterated isotopologues, where either the hydrogen (HCDO/ $H^{13}CDO$) or the deuterium (DCHO/ $D^{13}CHO$) dissociates or initiates the transition states and have thus been treated as two distinct isotopologues. The frequencies and zero-point vibrational energies of the S_0 state were calculated with CCSD(T)⁴²/aug-cc-pVTZ,^{43,44} the S_1 state with $\omega B97X-D$ ⁴⁵/aug-cc-pVTZ and the T_1 state with CASPT2^{46,47}/aug-cc-pVTZ. The CCSD(T) and CASPT2 calculations were performed using Molpro, 2020.2,⁴⁸ and the density functional theory calculations were performed using Gaussian 16.⁴⁹ The vibrational frequencies for HCHO were in good agreement with previous findings.^{23–26} The averages of the excitation energies and energy barriers from the literature^{23–27,33,50–58} were used and modified with the zero-point vibrational energies for the isotopologues determined in this study. Energy barriers, zero point energies, geometries and vibrational frequencies are available as electronic Supporting Information. The spin–orbit integrals were calculated for a $\omega B97X-D3(BJ)$ ⁵⁹/cc-pVTZ-optimized geometry of formaldehyde in vacuum to obtain the relevant spin–orbit coupling (SOC) value. The SOC was also computed using $\omega B97X-D3(BJ)$ /cc-pVTZ and was determined to be 0.007605 eV. Both the geometry optimization and SOC calculations were performed using ORCA (Release 5.0.1).⁶⁰

THEORY

The reaction rate coefficients for R3, R4, R6 and R7 (see Figure 1) have been determined as functions of wavelength

using Rice–Ramsperger–Kassel–Marcus (RRKM) theory.^{61–64} For a molecule with s oscillators with frequencies ν_i , the sum of states, $G(E)$, is given by⁶⁵

$$G(E) = \frac{(E + aE_z)^s}{s! \prod_{i=1}^s h\nu_i} \quad (6)$$

where E_z is the zero-point energy, and a has the limits of 0 and 1 for $E \rightarrow 0$ and $E \rightarrow \infty$, respectively. It is a function of $E' = E/E_z$ and the dispersion in the molecular vibrational frequencies

$$a = 1 - \beta\omega(E'), \quad \beta = \frac{s-1}{s} \frac{\langle \nu^2 \rangle}{\langle \nu \rangle^2} \quad (7)$$

where

$$\omega = [5.00E' + 2.73(E')^{0.50} + 3.51]^{-1} \quad (0.1 < E' < 1.0) \quad (8)$$

$$\omega = \exp[-2.4191(E')^{0.25}] \quad (1.0 < E' < 8.0) \quad (9)$$

The density of states, $N(E)$, is obtained by differentiating the sum of states $G(E)$

$$N(E) = \frac{(E + aE_z)^{s-1}}{(s-1)! \prod_{i=1}^s h\nu_i} \left[1 - \beta \frac{d\omega(E')}{dE'} \right] \quad (10)$$

The RRKM rate coefficient $K(E)$ is then given by

$$k(E) = \frac{1}{h} \frac{G(E^\ddagger)}{N(E_v)} \quad (11)$$

where $G(E^\ddagger)$ is the sum of states for the active degrees of freedom in the transition state, excluding the reaction coordinate, and $N(E_v)$ is the density of states for the active degrees of freedom in the reactant.

The relative rates of ISC (R2) and IC (R5) are determined using Fermi's Golden Rule,⁶⁶ assuming that the coupling only depends on the density of states. The density of states was calculated for each isotopologue and used to correct experimentally determined rates of ISC and IC.^{67,68}

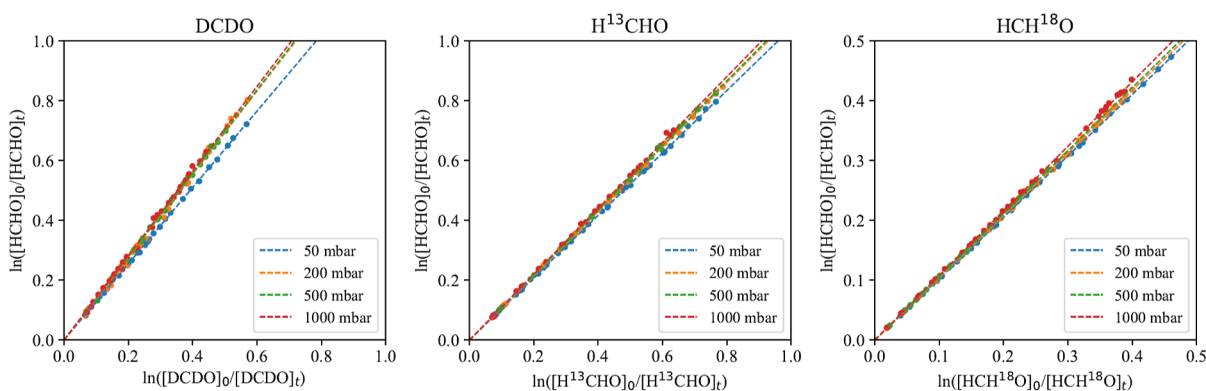


Figure 4. Relative rate experiments of HCHO versus DCDO, H¹³CHO and HCH¹⁸O at 50, 200, 500, and 1000 mbar pressure.

$$k_{\text{model, isotopologue}} = k_{\text{exp, HCHO}} \times \frac{N(E_{\nu})_{\text{heavy}}}{N(E_{\nu})_{\text{light}}} \quad (12)$$

The tunneling coefficients for R3, R4 and R7 were calculated using the 1D Eckart tunneling approach, where the Schrödinger equation is solved for an asymmetric one-dimensional Eckart potential.⁶⁹ For R3 and R4, the imaginary frequencies were calculated using $\omega\text{B97X-D/aug-cc-pVTZ}$, and the energy barriers were taken from the literature.^{23–26,33,50–55} The R7 tunneling coefficients were determined based on $\omega\text{B97X-D/aug-cc-pVTZ}$ intrinsic reaction coordinate (IRC) path geometries and energies, and were found to be insignificant. The tunneling coefficients were calculated for each reaction and for each isotopologue at five different temperatures: 288, 223, 218, 252, and 272 K, corresponding to 0, 10, 20, 30, 40, and 50 km altitude.¹

The collisional vibrational relaxation rates of the S₀, S₁ and T₁ states, $k_{\text{R8}} - k_{\text{R10}}$, were determined as functions of altitude by calculating the collision frequency. This involved assuming perfect gas behavior, that HCHO and N₂ have ellipsoidal shapes, and that every collision will result in sufficient loss of energy for the remaining reactions to be unable to occur. These rates have all been adjusted according to the difference in density of states relative to that of the ground state HCHO. Thus

$$z = \frac{N(E)_{\text{state, iso}}}{N(E)_{\text{S}_0, \text{HCHO}}} \times \frac{\sigma \nu_{\text{rel}} p}{kT}, \quad \nu_{\text{rel}} = \left(\frac{8RT}{\pi \mu} \right)^{1/2} \quad (13)$$

where σ is the collision cross-section of the molecules, ν_{rel} is the relative velocity and μ is the reduced mass of the molecules. The ellipsoidal collision cross-section is related to the spherical collision cross-section by

$$\frac{\sigma_{\text{spherical}}}{\sigma_{\text{ellipsoidal}}} = \ln \left(\frac{2a_1}{b_1} \right) \times \ln \left(\frac{2a_2}{b_2} \right) \quad (14)$$

where a_1 and b_1 are the length and width of HCHO and a_2 and b_2 are the length and width of N₂. These dimensions were determined by calculating the electron density surfaces of the molecules using Gaussian16 using $\omega\text{B97X-D/aug-cc-pVTZ}$ and the keyword “pop = chelpg”. The collisional vibrational relaxation rate of the T₁ state was adjusted using Fermi’s Golden Rule⁶⁶ and the SOC between the T₁ and S₀ states

$$k_{\text{R10}} = \frac{\text{SOC}_{\text{T}_1\text{S}_0}^2}{4\pi(kT)^2} \times k_{\text{R8}} \quad (15)$$

The rates for each isotopologue and each reaction were determined as a function of energy, corresponding to excitation wavelengths from 250 to 360 nm. As R2–R4 require an excitation to the S₁ state prior to reaction, the excitation energy of 337 kJ/mol was subtracted from the incoming energy. The experimental IC and ISC rates were approximated as being independent of energy, while the density of states was determined as functions of energy and used to adjust the IC and ISC rates. The unimolecular rates found for R7 are in agreement with the range of values found by Troe.⁷⁰

The quantum yields, $\Phi(E)$, of the entire process presented in Figure 1 can then be determined for the radical and molecular channels, as well as quenching to the S₀ state. This is done with the microcanonical reaction rates, $k(E)$, where the rates are functions of energy

$$\Phi_{\text{R}} = \frac{k_2 k_3}{N_{\text{S}_1} N_{\text{T}_1}} + \frac{k_4}{N_{\text{S}_1}} + \frac{k_5 k_6}{N_{\text{S}_1} N_{\text{S}_0^*}} \quad (16)$$

$$\Phi_{\text{M}} = \frac{k_5 k_7}{N_{\text{S}_1} N_{\text{S}_0^*}} \quad (17)$$

$$\Phi_{\text{S}_0} = \frac{k_8[M]}{N_{\text{S}_1}} + \frac{k_2 k_9[M]}{N_{\text{S}_1} N_{\text{T}_1}} + \frac{k_5 k_8[M]}{N_{\text{S}_1} N_{\text{S}_0^*}} \quad (18)$$

where

$$N_{\text{S}_0^*} = k_6 + k_7 + k_8[M] \quad (19)$$

$$N_{\text{S}_1} = k_2 + k_4 + k_5 + k_9[M] \quad (20)$$

$$N_{\text{T}_1} = k_3 + k_{10}[M] \quad (21)$$

The photolysis rate of an isotopologue is then found by multiplying the combined quantum yields of the radical and molecular channels with the absorption cross-section and light flux and integrating over the entire wavelength range

$$j = \int_{250}^{360} F(\lambda) (\Phi_{\text{R}}(\lambda) + \Phi_{\text{M}}(\lambda)) d\lambda \quad (22)$$

Gratien et al.¹⁹ have determined the absorption cross-section for DCHO and DCDO and the absorption cross sections for the remaining isotopologues have been approximated as that of HCHO. Thus, the KIE, α , of each isotopologue can be determined using the following equation

$$\alpha = \frac{j}{j'} \quad (23)$$

where j is the photolysis rate of HCHO and j' is the photolysis rate of a given isotopologue. The solar fluxes used throughout this paper have been modeled using the SMARTS2 (Version 2.9.2) Simple Model for Atmospheric Radiative Transmission of Sunshine of Gueymard.^{71,72} All spectra are modeled under the conditions of the Reference Air Mass 1.5 Spectra, unless stated otherwise.

RESULTS AND DISCUSSION

Experiments. The experiments were repeated three times at each pressure for DCDO, H¹³CHO and HCH¹⁸O. Less sample was available for DCHO; so these experiments were performed only once as single point determinations. The relative reaction rates for each experiment as well as all experiments at each pressure combined can be seen in Figure 4 and Table 2. For DCHO, $j_{\text{HCHO}}/j_{\text{DCHO}}$ was determined to be

Table 2. Experimental Relative Rates, $j_{\text{HCHO}}/j_{\text{DCDO}}$, $j_{\text{HCHO}}/j_{\text{H}^{13}\text{CHO}}$ and $j_{\text{HCHO}}/j_{\text{HCH}^{18}\text{O}}$, at Different Total Pressures

pressure/mbar	$j_{\text{HCHO}}/j_{\text{DCDO}}$	$j_{\text{HCHO}}/j_{\text{H}^{13}\text{CHO}}$	$j_{\text{HCHO}}/j_{\text{HCH}^{18}\text{O}}$
50	1.259 ± 0.075	1.044 ± 0.023	1.029 ± 0.011
50	1.268 ± 0.067	1.038 ± 0.012	1.022 ± 0.010
50	1.281 ± 0.035	1.044 ± 0.014	1.028 ± 0.010
50 _{all}	1.273 ± 0.034	1.042 ± 0.010	1.027 ± 0.006
200	1.386 ± 0.042	1.078 ± 0.016	1.043 ± 0.019
200	1.393 ± 0.300	1.072 ± 0.020	1.044 ± 0.021
200	1.404 ± 0.195	1.074 ± 0.030	1.043 ± 0.021
200 _{all}	1.388 ± 0.126	1.075 ± 0.012	1.044 ± 0.011
500	1.399 ± 0.067	1.087 ± 0.019	1.056 ± 0.018
500	1.396 ± 0.081	1.082 ± 0.023	1.052 ± 0.020
500	1.413 ± 0.196	1.085 ± 0.028	1.058 ± 0.008
500 _{all}	1.401 ± 0.051	1.085 ± 0.013	1.056 ± 0.009
1000	1.419 ± 0.087	1.114 ± 0.059	1.087 ± 0.034
1000	1.428 ± 0.181	1.096 ± 0.020	1.075 ± 0.020
1000	1.422 ± 0.249	1.097 ± 0.019	1.078 ± 0.024
1000 _{all}	1.418 ± 0.108	1.102 ± 0.022	1.080 ± 0.013

1.123 ± 0.030 , 1.130 ± 0.020 , 1.176 ± 0.011 and 1.166 ± 0.016 at 50, 200, 500, and 1000 mbar. The slopes and uncertainties were determined using a bivariate method presented by Cantrell,⁷³ where the uncertainties of the x - and y -values are based on the signal-to-noise ratio of the FTIR spectra and error propagation methods.

Figure 4 shows a pressure dependence for all species, where the KIEs increase with increasing pressure. However, this effect

is only statistically significant for all species when comparing 50 mbar to 500 and 1000 mbar, as well as for 200 mbar compared to 1000 mbar for HCH¹⁸O, see Table 2. The pressure dependence is smaller than that observed in previous experiments, due to the difference in lamp emission spectra.^{31,32} Residual plots were made for each pressure, as well as each experiment for DCDO, H¹³CHO and HCH¹⁸O, to investigate whether there are any systematic trends. No systematic residuals were found, see Supporting Information.

RRKM Model. The RRKM model is validated by comparison to experimental data from this study and from Nilsson et al.,^{31,32} (see Figure 5), which cover different excitation spectra and pressures, and using actinic flux at sea level and atmospheric pressure (see Figure 6). The xenon lamp

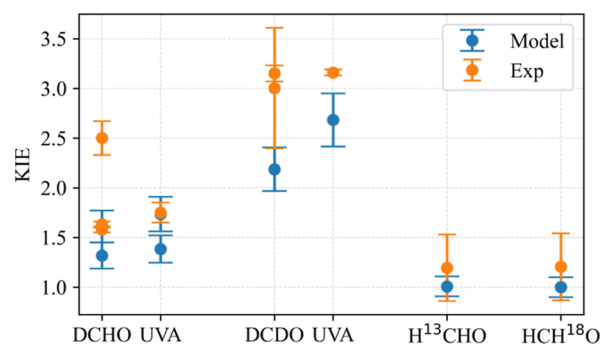


Figure 6. Modeled (blue) and experimental KIEs (orange) for DCHO, DCDO, H¹³CHO and HCH¹⁸O at 1030 mbar pressure and sea level actinic flux and UVA lamp if indicated. Experimental values are presented in Table 1.

allows investigation of high excitation energies, and the UVA lamp, low excitation energies. For the monodeuterated compounds, the model yields a range of KIEs, bounded by hydrogen (¹H) or deuterium (²H) transition states, see the two dashed blue lines in Figure 5 A and the two dashed purple lines in Figure 5 B. The uncertainty of the model is estimated to be 10% and is indicated by the shaded areas in Figure 5.

The model accurately predicts the KIEs for the deuterated species for both high and low excitation energies, and the results are within mutual uncertainties under most conditions. Furthermore, it accurately simulates the pressure trends at both high and low excitation energies. For an excitation spectrum relatively stronger at high energies the model systematically overestimates the KIEs (see Figure 5A). For

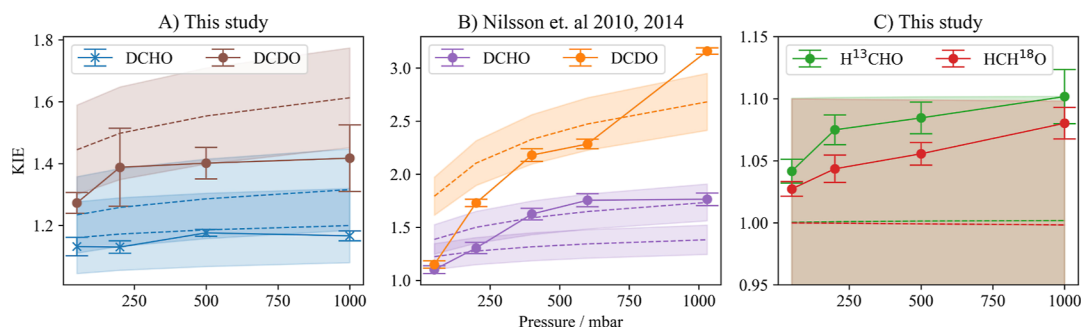


Figure 5. Modeled KIEs (dashed lines) compared to experimental KIEs (fully drawn lines) from this study, (A,C), and from Nilsson et al.,^{31,32} (B). For DCHO the model will present a range for the KIE, where the lower boundary is the hydrogen (¹H) dissociating or initiating transition states and the upper boundary is for deuterium (²H) as the active atom. The KIE of DCHO has only been determined experimentally as single points in this study and is distinguished with an \times . The uncertainty of the model is estimated as 10% and is represented by the shaded areas.

excitation biased to lower energies the model overestimates at low pressure and underestimates at high pressure (see Figure 5B).

While the modeled KIEs for H^{13}CHO and HCH^{18}O are consistently lower than the experimental values determined in this study and by Feilberg et al.,²⁹ they are within mutual uncertainties (see Figures 5C and 6). The systematic underestimation for these species could be due to non-RRKM behavior. The RRKM model is a statistical model that assumes that all states at a given energy are equally probable. However, the initial excitation is limited to an area of phase space corresponding to the Franck–Condon region and will approach the stochastic limit at a rate that may be slow relative to the lifetime of the species. The rate of randomization of the energy will depend on the internal motion of the system, which in turn is linked dynamically to the system's vibrational frequencies and symmetry. Clearly, isotopic substitution will change the vibrational frequencies. A heavier system with lower vibrational frequencies, higher vibrational quantum numbers and higher density of states will typically have faster randomization of the energy and will therefore have smaller deviations from the RRKM limit. A greater degree of non-RRKM behavior is expected for isotopically light systems. In addition, monodeutero systems will be better at randomizing energy than H_2 or D_2 isotopomers.

Inspection of the RRKM model results for the separate reactions can show why the pressure trends occur and which conditions will lead to the largest effects. Figure 7 shows the

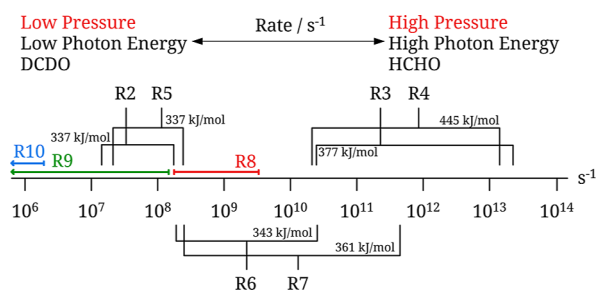


Figure 7. Range of reaction rates for the individual elementary reactions in formaldehyde photolysis. Competing reactions of S_1 (above x -axis), $S_0(\nu^*)$ (below x -axis) and collisional quenching (S_0 in red, S_1 in green and T_1 in blue). The rates have been determined as functions of pressure (1–1030 mbar) and photon energy (250–360 nm). The extremes of the range of rates are found for DCDO and HCHO with other isotopologues in between. The threshold energy for each reaction is shown in kJ/mol for HCHO.

calculated ranges of each reaction rate as functions of pressure, excitation energy and isotopic composition, with the competing reactions of the S_1 state above the x -axis, the competing reactions of the $S_0(\nu^*)$ state below the x -axis and the collision rate for the S_0 state in red, the S_1 state in green and the T_1 state in blue. A low excitation energy will result in a larger overlap between R6, R7 and R8. This will result in more competition between collisional quenching and dissociation of the $S_0(\nu^*)$ state, which explains why a larger pressure effect is observed in Nilsson et al.,^{31,32} than in this study (see Figure 2 for the lamp emission spectra). Furthermore, a heavier molecule will further increase the overlap between R6, R7 and R8, resulting in more competition, explaining the much larger pressure effect for DCDO than for DCHO seen in Figure 5 B.

This model is not suited to evaluate the wavelength dependence of the radical and molecular quantum yields. The system should be explored with reaction molecular dynamics calculations to establish any missing parts of the mechanism, as well as any other significant contributions to the quantum yields. For these investigations, we plan to perform ab initio multiple spawning (AIMS)^{74–76} interfaced with the TeraChem electronic structure program.^{77–81}

Predictions. Photochemical formation via formaldehyde is an important source of CO and H_2 —the two molecules that are formed in the molecular channel. Thus, isotope effects associated with formaldehyde photolysis have implications for the isotopic composition of these compounds; but the effects for the reactant and the product combined have rarely been studied together.

Having validated the model against all existing experimental data, we use it to predict the KIEs for the single and doubly deuterated species as functions of altitude (see Figure 8). As the model has been validated against both variations in pressure and light flux, it can be confidently used for this purpose. Modeling studies and measurements show increasing deuterium enrichment in molecular hydrogen with altitude, apparently due to altitude-dependent deuterium fractionation in the photochemical source of molecular hydrogen, i.e., formaldehyde photolysis.^{82–85} This is in line with the observed pressure trends found in this study and by Nilsson et al.^{31,32} However, the model shows that while the pressure effect is the main cause of the altitude dependence, observations at altitudes greater than 20 km can only be explained by also accounting for changes in the spectral distribution of sunlight.

Additionally, we suggest the model can be used to constrain the fraction of formaldehyde that deposits. The IPCC's Sixth Assessment Report (AR6)¹³ reports the direct and indirect radiative forcing of methane. The indirect radiative forcing is calculated by taking into account consequences of methane to atmospheric composition, such as formation of additional photochemical ozone, and CO_2 arising from CH_4 oxidation. The report assumes that 75% of methane is converted into CO_2 , while 25% is lost for example via deposition of formaldehyde, the important intermediate in the conversion of CH_4 to CO_2 . This approach builds on the Fifth Assessment Report (AR5),⁸⁶ which first included this indirect effect in its Global Warming Potential (GWP) and Global Temperature Potential (GTP) metrics for methane. If true, the deposition of formaldehyde to the surface is potentially a large carbon sink and one with important consequences. We note, however, that most OH is produced (and so, most CH_4 oxidized) in the middle and upper troposphere near the equator, far from the surface. This would suggest that 25% loss to deposition could be too high. An additional factor could be the loss of formaldehyde to aerosol particles, where it can become part of organic polymers.⁸⁷ A simple box model calculation with the isotope effects identified in this study, combined with field measurements of the abundance of ^{13}C and ^{18}O in carbon monoxide, could be used as an independent means of estimating the fraction of formaldehyde that is deposited.

CONCLUSIONS

The dependence of the relative rates of photolysis of H^{13}CHO , HCH^{18}O , DCHO and DCDO on pressure has been investigated experimentally. The trends due to pressure are in agreement with previous studies^{31,32} but cannot be directly

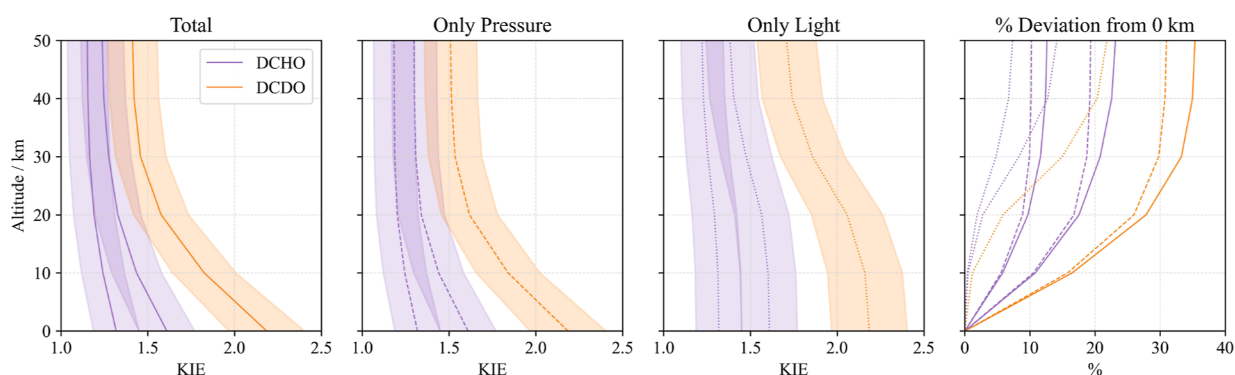


Figure 8. Predicted KIEs for DCHO (purple) and DCDO (orange) as a function of altitude, only effect of the pressure and only the effect of light flux, with 10% uncertainty indicated by the shaded areas. The last panel shows the percent deviation from the KIE at 0 km for the total effect (fully drawn), the pressure effect (dashed) and the light effect (dotted). For DCHO the model presents a range for the KIE, where the lower boundary is the hydrogen dissociating or initiating transition states and the upper boundary is for deuterium as the active atom. The solar flux was modeled at the various altitudes as described in the Theory section.

compared due to the difference in spectral distribution of the excitation sources.

The RRKM model is in excellent agreement with all experimental values and is within mutual uncertainties under most conditions. Furthermore, it accurately simulates the pressure trends at both high and low excitation energies. To further improve the model, the reaction paths need to be examined in greater detail. We plan to do this by performing ab initio multiple spawning trajectories interfaced with the TeraChem electronic structure program.

The model shows that the measured altitude-dependent deuterium enrichment in molecular hydrogen cannot be explained solely by the effect of pressure but must also include the wavelength dependence, especially at altitudes higher than 20 km.

■ ASSOCIATED CONTENT

SI Supporting Information

The Supporting Information is available free of charge at <https://pubs.acs.org/doi/10.1021/acs.jpca.4c07516>.

Energy barriers, zero point energies, geometries and vibrational frequencies for reactants, products and transition states along with residual plots for the experiments (PDF)

■ AUTHOR INFORMATION

Corresponding Author

Matthew S. Johnson – Department of Chemistry, University of Copenhagen, DK-2100 Copenhagen Ø, Denmark; orcid.org/0000-0002-3645-3955; Email: msj@chem.ku.dk

Authors

Luisa Pennacchio – Department of Chemistry, University of Copenhagen, DK-2100 Copenhagen Ø, Denmark

Zacharias Liasi – Department of Chemistry, University of Copenhagen, DK-2100 Copenhagen Ø, Denmark; orcid.org/0000-0001-6722-5640

Andreas Erbs Hillers-Bendtsen – Department of Chemistry, University of Copenhagen, DK-2100 Copenhagen Ø, Denmark; orcid.org/0000-0003-4960-8802

Thomas Röckmann – Institute for Marine and Atmospheric Research Utrecht (IMAU), 3584 CC Utrecht, The Netherlands; orcid.org/0000-0002-6688-8968

Kurt V. Mikkelsen – Department of Chemistry, University of Copenhagen, DK-2100 Copenhagen Ø, Denmark; orcid.org/0000-0003-4090-7697

Complete contact information is available at: <https://pubs.acs.org/10.1021/acs.jpca.4c07516>

Author Contributions

Conceptualization, MSJ, TR, KVM; Data Curation, LP; Formal Analysis, LP; Funding Acquisition, MSJ; Investigation, LP; Methodology, LP, ZL, AEHB, KVM, MSJ; Project Administration, KVM, MSJ; Resources, KVM, MSJ; Software, LP, ZL, AEHB, KVM; Supervision, KVM, MSJ; Validation, LP; Visualization, LP; Writing – Original Draft, LP; Writing – Review & Editing, LP, ZL, AEHB, TR, KVM, MSJ.

Notes

The authors declare no competing financial interest.

■ ACKNOWLEDGMENTS

The work was supported by Spark Climate Solutions and ACTRIS-DK.

■ REFERENCES

- Seinfeld, J. H.; Pandis, S. N. *Atmospheric Chemistry and Physics: From Air Pollution to Climate Change*; John Wiley & Sons, 2016.
- Novelli, P.; Lang, P.; Masarie, K.; Hurst, D.; Myers, R.; Elkins, J. Molecular hydrogen in the troposphere: Global distribution and budget. *J. Geophys. Res.* **1999**, *104*, 30427–30444.
- Röckmann, T.; Gómez Alvarez, C. X.; Walter, S.; van der Veen, C.; Wollny, A. G.; Gunthe, S. S.; Helas, G.; Pöschl, U.; Keppler, F.; Greule, M.; Brand, W. A. Isotopic composition of H₂ from wood burning: Dependency on combustion efficiency, moisture content, and Delta D of local precipitation. *J. Geophys. Res.: Atmos.* **2010**, *115*, 1–11.
- Ehhalt, D. H.; Rohrer, F. The tropospheric cycle of H₂: a critical review. *Tellus B* **2022**, *61*, 500–535.
- Rhee, T. S.; Brenninkmeijer, C. A. M.; Röckmann, T. Hydrogen isotope fractionation in the photolysis of formaldehyde. *Atmos. Chem. Phys.* **2008**, *8*, 1353–1366.
- Forster, P.; Ramaswamy, V.; Artaxo, P.; Berntsen, T.; Betts, R.; Fahey, D. W.; Haywood, J.; Lean, J.; Lowe, D. C.; Myhre, G.; et al. Changes in atmospheric constituents and in radiative forcing. *Climate Change 2007: The Physical Science Basis. Contribution of Working Group I to the 4th Assessment Report of the Intergovernmental Panel on Climate Change*, 2007; pp 131–217.

- (7) Schultz, M. G.; Diehl, T.; Brasseur, G. P.; Zittel, W. Air Pollution and Climate-Forcing Impacts of a Global Hydrogen Economy. *Science* **2003**, *302*, 624–627.
- (8) Tromp, T. K.; Shia, R.-L.; Allen, M.; Eiler, J. M.; Yung, Y. L. Potential Environmental Impact of a Hydrogen Economy on the Stratosphere. *Science* **2003**, *300*, 1740–1742.
- (9) Warwick, N. J.; Bekki, S.; Nisbet, E. G.; Pyle, J. A. Impact of a hydrogen economy on the stratosphere and troposphere studied in a 2-D model. *Geophys. Res. Lett.* **2004**, *31*, 1–4.
- (10) Hauglustaine, D.; Paulot, F.; Collins, W.; Derwent, R.; Sand, M.; Boucher, O. Climate benefit of a future hydrogen economy. *Commun. Earth Environ.* **2022**, *3*, 295.
- (11) Ocko, I. B.; Hamburg, S. P. Climate consequences of hydrogen emissions. *Atmos. Chem. Phys.* **2022**, *22*, 9349–9368.
- (12) Pieterse, G.; et al. Reassessing the variability in atmospheric H₂ using the two-way nested TMS model. *J. Geophys. Res.: Atmos.* **2013**, *118*, 3764–3780.
- (13) *Climate Change 2023: Synthesis Report. Contribution of Working Groups I, II and III to the Sixth Assessment Report of the Intergovernmental Panel on Climate Change*; Team, C. W., Lee, H., Romero, J., Eds.; IPCC: Geneva, Switzerland, 2023; pp 35–115.
- (14) Bergamaschi, P.; Hein, R.; Brenninkmeijer, C. A. M.; Crutzen, P. J. Inverse modeling of the global CO cycle: 2. Inversion of ¹³C/¹²C and ¹⁸O/¹⁶O isotope ratios. *J. Geophys. Res.: Atmos.* **2000**, *105*, 1929–1945.
- (15) Zheng, B.; Chevallier, F.; Yin, Y.; Ciais, P.; Fortems-Cheiney, A.; Deeter, M. N.; Parker, R. J.; Wang, Y.; Worden, H. M.; Zhao, Y. Global atmospheric carbon monoxide budget 2000–2017 inferred from multi-species atmospheric inversions. *Earth Syst. Sci. Data* **2019**, *11*, 1411–1436.
- (16) Jang, M.; Kamens, R. M. Atmospheric secondary aerosol formation by heterogeneous reactions of aldehydes in the presence of a sulfuric acid aerosol catalyst. *Environ. Sci. Technol.* **2001**, *35*, 4758–4766.
- (17) van Herpen, M. M.; Li, Q.; Saiz-Lopez, A.; Liisberg, J. B.; Röckmann, T.; Cuevas, C. A.; Fernandez, R. P.; Mak, J. E.; Mahowald, N. M.; Hess, P.; et al. Photocatalytic chlorine atom production on mineral dust–sea spray aerosols over the North Atlantic. *Proc. Natl. Acad. Sci. U.S.A.* **2023**, *120*, No. e2303974120.
- (18) Burkholder, J. B.; Sander, S. P.; Abbatt, J. P. D.; Barker, J. R.; Cappa, C.; Crounse, J. D.; Dibble, T. S.; Huie, R. E.; Kolb, C. E.; Kurylo, M. J.; et al. *Chemical Kinetics and Photochemical Data for Use in Atmospheric Studies Evaluation Number 19 NASA Panel for Data Evaluation*, 2020.
- (19) Gratién, A.; Nilsson, E.; Doussin, J.-F.; Johnson, M. S.; Nielsen, C. J.; Stenström, Y.; Picquet-Varrault, B. UV and IR Absorption Cross-sections of HCHO, HCDO, and DCDO. *J. Phys. Chem. A* **2007**, *111*, 11506–11513.
- (20) Gratién, A.; Picquet-Varrault, B.; Orphal, J.; Perraudin, E.; Doussin, J.-F.; Flaud, J.-M. Laboratory intercomparison of the formaldehyde absorption cross sections in the infrared (1660–1820 cm⁻¹) and ultraviolet (300–360 nm) spectral regions. *J. Geophys. Res.: Atmos.* **2007**, *112*, 1–10.
- (21) Tatum Ernest, C.; Bauer, D.; Hynes, A. J. High-Resolution Absorption Cross Sections of Formaldehyde in the 30285–32890 cm⁻¹ (304–330 nm) Spectral Region. *J. Phys. Chem. A* **2012**, *116*, 5910–5922.
- (22) Rogers, J. D. Ultraviolet absorption cross sections and atmospheric photodissociation rate constants of formaldehyde. *J. Phys. Chem.* **1990**, *94*, 4011–4015.
- (23) Maeda, S.; Ohno, K.; Morokuma, K. Automated global mapping of minimal energy points on seams of crossing by the anharmonic downward distortion following method: A case study of H₂CO. *J. Phys. Chem. A* **2009**, *113*, 1704–1710.
- (24) Guan, Y.; Xie, C.; Guo, H.; Yarkony, D. R. Enabling a Unified Description of Both Internal Conversion and Intersystem Crossing in Formaldehyde: A Global Coupled Quasi-Diabatic Hamiltonian for Its S₀, S₁, and T₁ States. *J. Chem. Theory Comput.* **2021**, *17*, 4157–4168.
- (25) Fu, B.; Shepler, B. C.; Bowman, J. M. Three-State Trajectory Surface Hopping Studies of the Photodissociation Dynamics of Formaldehyde on ab Initio Potential Energy Surfaces. *J. Am. Chem. Soc.* **2011**, *133*, 7957–7968.
- (26) Zhang, P.; Maeda, S.; Morokuma, K.; Braams, B. J. Photochemical reactions of the low-lying excited states of formaldehyde: T₁/S₁ intersystem crossings, characteristics of the S₁ and T₁ potential energy surfaces, and a global T₁ potential energy surface. *J. Chem. Phys.* **2009**, *130*, 114304.
- (27) Townsend, D.; Lahankar, S. A.; Lee, S. K.; Chambreau, S. D.; Suits, A. G.; Zhang, X.; Rheinecker, J.; Harding, L. B.; Bowman, J. M. The Roaming Atom: Straying from the Reaction Path in Formaldehyde Decomposition. *Science* **2004**, *306*, 1158–1161.
- (28) Feilberg, K. L.; Johnson, M. S.; Bacak, A.; Röckmann, T.; Nielsen, C. J. Relative Tropospheric Photolysis Rates of HCHO and HCDO Measured at the European Photoreactor Facility. *J. Phys. Chem. A* **2007**, *111*, 9034–9046.
- (29) Feilberg, K. L.; D’Anna, B.; Johnson, M. S.; Nielsen, C. J. Relative Tropospheric Photolysis Rates of HCHO, H₁₃CHO, HCH₁₈O, and DCDO Measured at the European Photoreactor Facility. *J. Phys. Chem. A* **2005**, *109*, 8314–8319.
- (30) Nilsson, E. J. K.; Bache-Andreassen, L.; Johnson, M. S.; Nielsen, C. J. Relative Tropospheric Photolysis Rates of Acetaldehyde and Formaldehyde Isotopologues Measured at the European Photoreactor Facility. *J. Phys. Chem. A* **2009**, *113*, 3498–3504.
- (31) Nilsson, E. J. K.; Andersen, V. F.; Skov, H.; Johnson, M. S. Pressure dependence of the deuterium isotope effect in the photolysis of formaldehyde by ultraviolet light. *Atmos. Chem. Phys.* **2010**, *10*, 3455–3462.
- (32) Nilsson, E. J. K.; Schmidt, J. A.; Johnson, M. S. Pressure dependent isotopic fractionation in the photolysis of formaldehyde-d₂. *Atmos. Chem. Phys.* **2014**, *14*, 551–558.
- (33) Moore, C. B.; Weisshaar, J. C. Formaldehyde Photochemistry. *Annu. Rev. Phys. Chem.* **1983**, *34*, 525–555.
- (34) Houston, P. L.; Moore, C. B. Formaldehyde photochemistry: Appearance rate, vibrational relaxation, and energy distribution of the CO product. *J. Chem. Phys.* **1976**, *65*, 757–770.
- (35) Ho, P.; Bamford, D. J.; Buss, R. J.; Lee, Y. T.; Moore, C. B. Photodissociation of formaldehyde in a molecular beam. *J. Chem. Phys.* **1982**, *76*, 3630–3636.
- (36) Yeung, E. S.; Moore, C. B. Predissociation model for formaldehyde. *J. Chem. Phys.* **1974**, *60*, 2139–2147.
- (37) Polik, W. F.; Guyer, D. R.; Moore, C. B. Stark level-crossing spectroscopy of S formaldehyde eigenstates at the dissociation threshold. *J. Chem. Phys.* **1990**, *92*, 3453–3470.
- (38) Troe, J. Refined analysis of the thermal dissociation of formaldehyde. *J. Phys. Chem. A* **2007**, *111*, 3862–3867.
- (39) Weisshaar, J. C.; Moore, C. B. Isotope, electric field, and vibrational state dependence of single rotational level lifetimes of S₁ formaldehyde. *J. Chem. Phys.* **1980**, *72*, 5415–5425.
- (40) Welsh, B. A.; Corrigan, M. E.; Assaf, E.; Nauta, K.; Sebastianelli, P.; Jordan, M. J.; Fittschen, C.; Kable, S. H. Photophysical oxidation of HCHO produces HO₂ radicals. *Nat. Chem.* **2023**, *15*, 1350–1357.
- (41) Bruker Optik GmbH. *OPUS 7.0 Software*, 2012. <https://www.bruker.com>.
- (42) Watts, J. D.; Gauss, J.; Bartlett, R. J. Coupled-cluster methods with noniterative triple excitations for restricted open-shell Hartree–Fock and other general single determinant reference functions. Energies and analytical gradients. *J. Chem. Phys.* **1993**, *98*, 8718–8733.
- (43) Dunning, T. H. Gaussian Basis Sets for Use in Correlated Molecular Calculations. I. The Atoms Boron Through Neon and Hydrogen. *J. Chem. Phys.* **1989**, *90*, 1007–1023.
- (44) Kendall, R. A.; Dunning, T. H., Jr; Harrison, R. J.; Harrison, R. J. Electron affinities of the first-row atoms revisited. Systematic basis sets and wave functions. *J. Chem. Phys.* **1992**, *96*, 6796–6806.
- (45) Chai, J. D.; Head-Gordon, M. Long-range corrected hybrid density functionals with damped atom-atom dispersion corrections. *Phys. Chem. Chem. Phys.* **2008**, *10*, 6615–6620.

- (46) Andersson, K.; Malmqvist, P. A.; Roos, B. O.; Sadlej, A. J.; Wolinski, K. Second-order perturbation theory with a CASSCF reference function. *J. Phys. Chem.* **1990**, *94*, 5483–5488.
- (47) Andersson, K.; Malmqvist, P. Å.; Roos, B. O. Second-order perturbation theory with a complete active space self-consistent field reference function. *J. Chem. Phys.* **1992**, *96*, 1218–1226.
- (48) Werner, H.-J.; Knowles, P. J.; Knizia, G.; Manby, F. R.; Schütz, M.; Celani, P.; Györffy, W.; Kats, D.; Korona, T.; Lindh, R.; et al. *MOLPRO*, version 2012.1, A package of ab initio programs, 2012.
- (49) Frisch, M. J.; Trucks, G. W.; Schlegel, H. B.; Scuseria, G. E.; Robb, M. A.; Cheeseman, J. R.; Scalmani, G.; Barone, V.; Petersson, G. A.; Nakatsuji, H.; et al. *Gaussian 16*. Revision A.01; Gaussian Inc: Wallingford CT, 2016.
- (50) Gelbart, W. M.; Elert, M. L.; Heller, D. F. Photodissociation of the formaldehyde molecule: does it or doesn't it? *Chem. Rev.* **1980**, *80*, 403–416.
- (51) Green, W. H.; Moore, C. B.; Polik, W. F. Transition States and Rate Constants for Unimolecular Reactions. *Annu. Rev. Phys. Chem.* **1992**, *43*, 591–626.
- (52) Dulligan, M.; Tuchler, M.; Zhang, J.; Kolessov, A.; Wittig, C. HCO rotational excitation in the photoinitiated unimolecular decomposition of H₂CO. *Chem. Phys. Lett.* **1997**, *276*, 84–91.
- (53) Palke, W. E.; Kirtman, B. The C-H bond energy of formaldehyde. *Chem. Phys. Lett.* **1988**, *148*, 202–204.
- (54) Adams, G. F.; Bent, G. D.; Bartlett, R. J.; Purvis, G. D. Formaldehyde: Electronic structure calculations for the S and T 1 states. *J. Chem. Phys.* **1981**, *75*, 834–842.
- (55) Frisch, M.; Krishnan, R.; Pople, J. The lowest singlet potential surface of formaldehyde. *J. Phys. Chem.* **1981**, *85*, 1467–1468.
- (56) Terentis, A. C.; Kable, S. H. Near threshold dynamics and dissociation energy of the reaction H₂CO → HCO + H. *Chem. Phys. Lett.* **1996**, *258*, 626–632.
- (57) Feller, D.; Dupuis, M.; Garrett, B. C. Barrier for the H₂CO → H₂+CO reaction: A discrepancy between high-level electronic structure calculations and experiment. *J. Chem. Phys.* **2000**, *113*, 218–226.
- (58) Polik, W. F.; Guyer, D. R.; Moore, C. B. Stark level-crossing spectroscopy of S formaldehyde eigenstates at the dissociation threshold. *J. Chem. Phys.* **1990**, *92*, 3453–3470.
- (59) Najibi, A.; Goerigk, L. The Nonlocal Kernel in van der Waals Density Functionals as an Additive Correction: An Extensive Analysis with Special Emphasis on the B97M-V and ωB97M-V Approaches. *J. Chem. Theory Comput.* **2018**, *14*, 5725–5738.
- (60) Neese, F. The ORCA program system. *Wiley Interdiscip. Rev.: Comput. Mol. Sci.* **2012**, *2*, 73–78.
- (61) Rice, O. K.; Ramsperger, H. C. Theories of unimolecular gas reactions at low pressures. *J. Am. Chem. Soc.* **1927**, *49*, 1617–1629.
- (62) Kassel, L. S. Studies in homogeneous gas reactions. I. *J. Phys. Chem.* **1928**, *32*, 225–242.
- (63) Marcus, R. A.; Rice, O. The Kinetics of the Recombination of Methyl Radicals and Iodine Atoms. *J. Phys. Chem.* **1951**, *55*, 894–908.
- (64) Marcus, R. Dissociation and isomerization of vibrationally excited species. III. *J. Chem. Phys.* **1965**, *43*, 2658–2661.
- (65) Whitten, G.; Rabinovitch, B. Accurate and facile approximation for vibrational energy-level sums. *J. Chem. Phys.* **1963**, *38*, 2466–2473.
- (66) Atkins, P.; Friedman, R. *Molecular Quantum Mechanics*, 4th ed.; OUP Oxford, 2011; pp 193–196.
- (67) Chuang, M.; Foltz, M. F.; Moore, C. B. T1 barrier height, S1–T1 intersystem crossing rate, and S0 radical dissociation threshold for H₂CO, D₂CO, and HD₂CO. *J. Chem. Phys.* **1987**, *87*, 3855–3864.
- (68) Miller, R. G.; Lee, E. K. C. Single vibronic level photochemistry of formaldehydes in the \tilde{A}^1A_2 state: Radiative and nonradiative processes in H₂CO, HD₂CO, and D₂CO. *J. Chem. Phys.* **1978**, *68*, 4448–4464.
- (69) Eckart, C. The penetration of a potential barrier by electrons. *Phys. Rev.* **1930**, *35*, 1303–1309.
- (70) Troe, J. Analysis of quantum yields for the photolysis of formaldehyde at λ 310 nm. *J. Phys. Chem. A* **2007**, *111*, 3868–3874.
- (71) Guemard, C. A. Parameterized transmittance model for direct beam and circumsolar spectral irradiance. *Sol. Energy* **2001**, *71*, 325–346.
- (72) Guemard, C.; Myers, D.; Emery, K. Proposed reference irradiance spectra for solar energy systems testing. *Sol. Energy* **2002**, *73*, 443–467.
- (73) Cantrell, C. A. Technical Note: Review of methods for linear least-squares fitting of data and application to atmospheric chemistry problems. *Atmos. Chem. Phys.* **2008**, *8*, 5477–5487.
- (74) Ben-Nun, M.; Quenneville, J.; Martinez, T. J. Ab initio multiple spawning: Photochemistry from first principles quantum molecular dynamics. *J. Phys. Chem. A* **2000**, *104*, 5161–5175.
- (75) Ben-Nun, M.; Martinez, T. J. Ab initio quantum molecular dynamics. *Adv. Chem. Phys.* **2002**, *121*, 439–512.
- (76) Ben-Nun, M.; Martinez, T. J. Nonadiabatic molecular dynamics: Validation of the multiple spawning method for a multidimensional problem. *J. Chem. Phys.* **1998**, *108*, 7244–7257.
- (77) Seritan, S.; Bannwarth, C.; Fales, B. S.; Hohenstein, E. G.; Kokkila-Schumacher, S. I. L.; Luehr, N.; Snyder, J. W., Jr; Song, C.; Titov, A. V.; Ufimtsev, I. S.; et al. TeraChem: Accelerating electronic structure and ab initio molecular dynamics with graphical processing units. *J. Chem. Phys.* **2020**, *152*, 224110.
- (78) Ufimtsev, I. S.; Martinez, T. J. Quantum Chemistry on Graphical Processing Units. 1. Strategies for Two-Electron Integral Evaluation. *J. Chem. Theory Comput.* **2008**, *4*, 222–231.
- (79) Ufimtsev, I. S.; Martinez, T. J. Quantum Chemistry on Graphical Processing Units. 3. Analytical Energy Gradients, Geometry Optimization, and First Principles Molecular Dynamics. *J. Chem. Theory Comput.* **2009**, *5*, 2619–2628.
- (80) Ufimtsev, I. S.; Martinez, T. J. Quantum Chemistry on Graphical Processing Units. 2. Direct Self-Consistent-Field Implementation. *J. Chem. Theory Comput.* **2009**, *5*, 1004–1015.
- (81) Seritan, S.; Ufimtsev, I. S.; Martinez, T. J.; et al. A graphical processing unit-accelerated electronic structure package for large-scale ab initio molecular dynamics. *Wiley Interdiscip. Rev.: Comput. Mol. Sci.* **2021**, *11*, No. e1494.
- (82) Röckmann, T.; Rhee, T. S.; Engel, A. Heavy hydrogen in the stratosphere. *Atmos. Chem. Phys.* **2003**, *3*, 2015–2023.
- (83) Mar, K. A.; McCarthy, M. C.; Connell, P.; Boering, K. A. Modeling the photochemical origins of the extreme deuterium enrichment in stratospheric H₂. *J. Geophys. Res.: Atmos.* **2007**, *112*, 1–24.
- (84) Pieterse, G.; Krol, M. C.; Batenburg, A. M.; Steele, L. P.; Krummel, P. B.; Langenfelds, R. L.; Röckmann, T. Global modelling of H₂ mixing ratios and isotopic compositions with the TMS model. *Atmos. Chem. Phys.* **2011**, *11*, 7001–7026.
- (85) Batenburg, A. M.; Schuck, T. J.; Baker, A. K.; Zahn, A.; Brenninkmeijer, C. A. M.; Röckmann, T. The stable isotopic composition of molecular hydrogen in the tropopause region probed by the CARIBIC aircraft. *Atmos. Chem. Phys.* **2012**, *12*, 4633–4646.
- (86) *Climate Change 2014: Synthesis Report. Contribution of Working Groups I, II and III to the Fifth Assessment Report of the Intergovernmental Panel on Climate Change*; Core Writing Team, R. K. P.; Meyer, L. A., Eds.; IPCC: Geneva, Switzerland, 2014; pp 1–151.
- (87) Xu, R.; et al. Field observations and quantifications of atmospheric formaldehyde partitioning in gaseous and particulate phases. *Sci. Total Environ.* **2022**, *808*, 152122.